RESEARCH ARTICLE

An Energy-Tunable Dual Emission Mechanism of the Hybridized Local and Charge Transfer (HLCT) and the Excited State Conjugation Enhancement (ESCE)

Kensuke Suga,[a,b] Keisuke Ochiai,[c,d] Yusuke Yoneda[c,d], Hikaru Kuramochi,*[c,d] and Shohei Saito*[b]

[a] K. Suga,
Department of Chemistry, Graduate School of Science, Kyoto University,
Kitashirakawa Oiwake-cho, Sakyo-ku, Kyoto, Kyoto 606-8502 (Japan),
[b] K. Suga, Prof. Dr. S. Saito,
Department of Chemistry, Graduate School of Science, Osaka University,
1-1 Machikaneyama-cho, Toyonaka, Osaka 560-0043 (Japan),
[c] K. Ochiai, Dr. Y. Yoneda, Prof. Dr. H. Kuramochi,
Research Center of Integrative Molecular Systems (CIMoS),
Institute for Molecular Science, National Institutes of Natural Sciences,
38 Nishigo-Naka, Myodaiji, Okazaki, Aichi 444-8585 (Japan)
[d] K. Ochiai, Dr. Y. Yoneda, Prof. Dr. H. Kuramochi,
Graduate Institute for Advanced Studies, SOKENDAI,
38 Nishigo-Naka, Myodaiji, Okazaki, Aichi 444-8585 (Japan)

E-mail: saito.shohei@chem.sci.osaka-u.ac.jp, hkuramochi@ims.ac.jp

Supporting information for this article is given via a link at the end of the document.

Abstract: Molecular design of dual-fluorescent probes requires precise adjustment of the energy levels of two excited states and the energy barrier between them. While the hybridized local and charge-transfer (HLCT) state has been recently focused as an important excited state for high emission efficiency with a tunable energy level, a dual emission involving the HLCT state has been only achieved with the excited-state intramolecular proton transfer (ESIPT) system. Here, a series of dual-fluorescent molecules involving an HLCT excited state with the excited-state conjugation enhancement (ESCE) motif is presented as the first case. The energy level of the HLCT state has been adjusted by changing substituents and solvents, separately from the ESCE energy level. The HLCT-ESCE molecular design with tunable fluorescence properties proposes a new strategy for the development of advanced fluorescent probes.

Introduction

Dual emission has attracted considerable attention in molecular photochemistry due to a variety of mechanisms and the related applications.[1] With an environment-sensitive dual-fluorescent probe,[2,3] ratiometric analysis can be performed by evaluating the intensity ratio of two emission bands, which enables quantitative environment imaging regardless of inhomogeneous distribution of the probe molecules.[4,5] In addition to the vital role in sensing ions[6,7] and chemical species,[8,9] dual-emissive molecules are useful tools for probing local viscosity,[10] temperature,[11,12] pH,[13] or tension[14–16] in complex soft matter such as living cells[17–20] and network polymers.[21–25] Combinational use with a confocal microscope or a hyperspectral camera allows quantitative microenvironment imaging with a simpler setup than the fluorescence lifetime imaging (FLIM).[26–30]

As representative cases, dual emissive biosensors based on the Förster resonance energy transfer (FRET) mechanism are widely used for detecting microenvironments,[31,32] while dual emissive excited-state intramolecular proton transfer (ESIPT) fluorescent probes are used as chemosensors.[33] The key to achieving dual-fluorescence is the design of molecules that exhibit a significant structural change in the excited state as well as an instant reversibility in the ground state (Figure 1a). A variety of strategies have been employed to induce the large structural change, including twisted/planarized intramolecular charge transfer (TICT/PLICT),[34–39] excimer formation in a fluorophore dimer,[40–42] and excited-state conjugate enhancement (ESCE).[43–46] In particular, a large conformational change caused by ESCE provides a function of advanced fluorescent probes for real-time materials imaging. Our group has developed the flexible and aromatic photofunctional system (FLAP)[47] as a platform for probing nanoscale environments through a molecular flapping motion. In the ground state, FLAP takes a V-shaped, bent conformation as the most stable geometry. When subjected to environments with limited free volume, FLAP almost maintains the V-shaped conformation and typically emits a blue fluorescence from the first singlet excited state (S_1) (Figure 1b). Conversely, under conditions with sufficient free volume, FLAP changes the conformation to a planar geometry, which typically results in a green fluorescence from S_1. The dual emission is induced by altering the electronic configuration, classified as an ESCE system.[1] With this property, FLAP serves as a fluorescent probe for a diverse range of applications, such as viscosity probes,[48–50] free volume probes for polymeric materials,[51] and force probes for mechanochemistry and soft matter physics.[52–54]

Tuning the excited state potential energy surface is important for the versatility of dual-emissive fluorophores. Modulation of the donor-acceptor design for photoinduced electron transfer[55–58] is a major approach to manipulate the excited-state energy surface, with other strategies involving the introduction of steric hindrance[59–65] and excited-state aromaticity.[66] In particular, tuning the excited-state energy level of the ESCE systems has been reported by introducing a charge transfer (CT) moiety into dibenzo[*b*,*f*]azepine,[67]

tribenzo[*b*,*d*,*f*]azepine,[68] and *N*,*N*'-diaryl-dihydrodibenzo[*a*,*e*]phenazine systems.[69] The energy level of the CT state can be readily tuned by substituents and surrounding environments, such as solvent polarity. However, the CT state exhibits a smaller orbital overlap between HOMO and LUMO, which results in a decreased oscillator strength (*f*) of the lowest-energy transition. The small oscillator strength leads to a lower absorption efficiency and a lower radiative decay rate, which diminishes the performance of fluorescent probes. Several strategies have been developed to increase the orbital overlap in the CT transition. The use of D-π-A motifs is one of the representative approaches to solving the problem of a low oscillator strength, often used in dye-sensitized solar cells.[70] Another approach is to hybridize the locally excited state with the CT state, called the HLCT excited state (Figure 1c). The HLCT state is characterized by each contribution of the highly emissive LE state and the CT state with the tunable energy level.[71–74] Molecules with the HLCT excited state have been employed as emitters in organic light-emitting diodes (OLEDs)[75] and have also been utilized as chemosensors.[76,77] Although the HLCT excited state has been incorporated into the ESIPT dual emission systems,[78,79] the adoption of the HLCT state in the ESCE dual emission system has not been reported.

Here, we report a strategy to design a characteristic molecule that shows dual fluorescence from the HLCT state and the ESCE state. To construct the HLCT system **Wing1a–d**, the phenazine skeleton was combined with *para*-substituted phenyl groups with different substituents (Figure 1d). Furthermore, this HLCT system was embedded in the "flapping wings" of the previously reported N-FLAP molecules (**FLAP1a–d**), thereby enabling the tunable dual fluorescence.

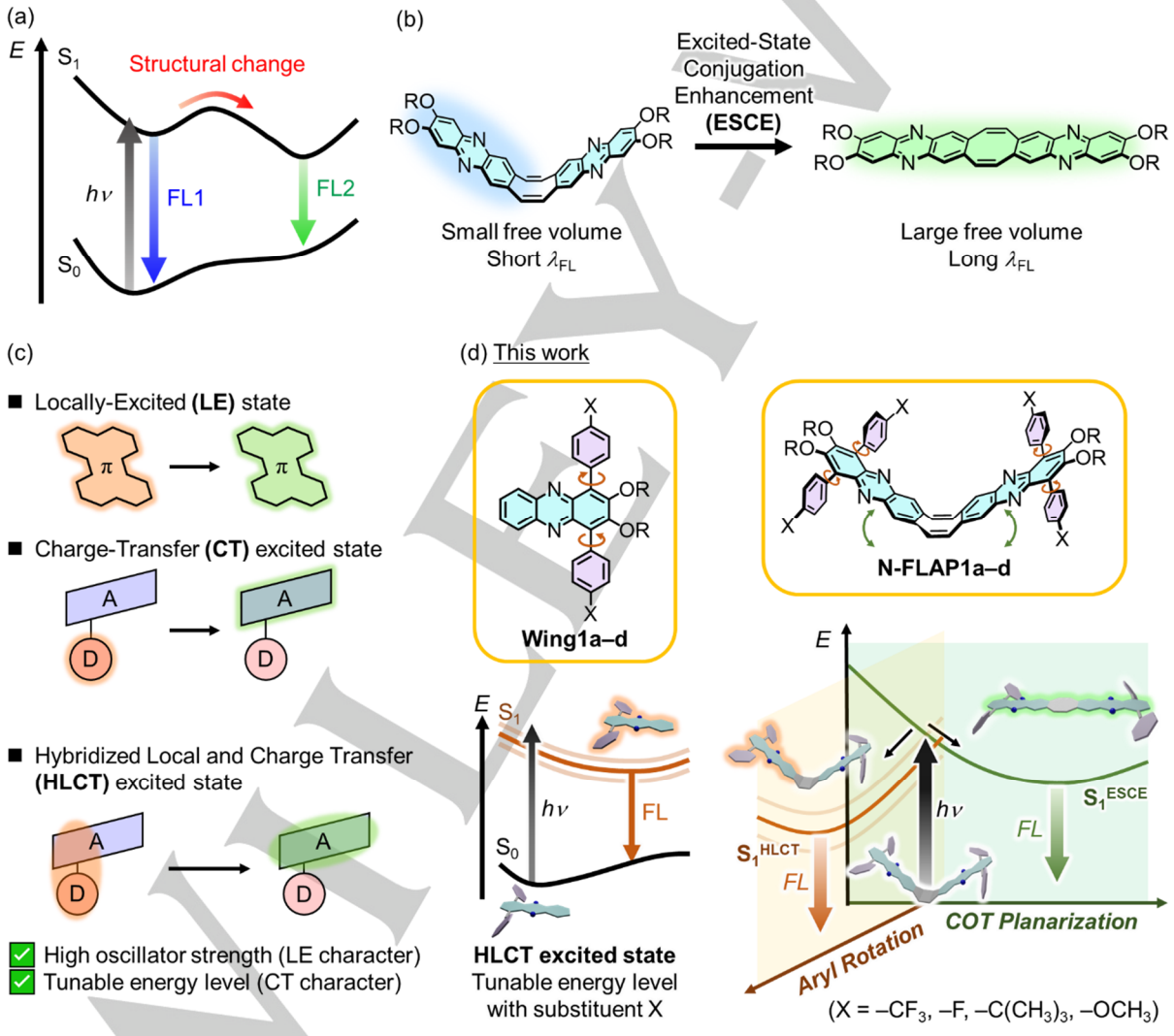

Figure 1. (a) Ground-state and excited-state energy diagram of dual-fluorescent molecules. (b) The previously reported N-FLAP molecule showing a dual fluorescence from V-shaped and planar conformations. (c) Characteristics of an HLCT excited state compared to an LE state and a CT excited state. D: Donor, A: Acceptor. (d) Combination of a phenazine core and *para*-substituted phenyl groups yielded **Wing1a–d** exhibiting an HLCT excited state. The substituted phenazine moiety has been introduced as the "flapping wings" of N-FLAP (**N-FLAP1a–d**) to achieve dual fluorescence from the HLCT and ESCE states. The fluorescence wavelength of the HLCT emission can be tuned by the electronic modulation of the substituents.

Results and Discussion

Construction of an HLCT unit in substituted phenazines

The synthesis of **Wing1a–d** and the V-shaped dimers **N-FLAP1a–d** is shown in Figure 2a. Key precursors **Wing3** and **N-FLAP3** were prepared by bromination of 2,3-dihexyloxyphenazine (**Wing2**) and corresponding FLAP (**N-FLAP2**)[51,54] with *N*-bromosuccinimide (NBS)[80,81] in 89% and 82% yield, respectively. Suzuki coupling of these products with *para*-substituted phenylboronic acids to afford the corresponding HLCT units **Wing1a–d** from **Wing3** in 95–100% yield, and **N-FLAP1a–d** from **N-FLAP3** in 75–77% yield. The late-step substitution allowed easy modulation of the photophysical properties of the phenazine and N-FLAP derivatives. X-ray crystal structures of **N-FLAP1a–d** showed V-shaped bent geometries, taking the COT bending angle of 40.0–48.5° (Figure 2b and S35 to S38), indicating that the most stable conformation of the aryl substituted N-FLAP molecules is bent, as reported in the unsubstituted ones.[51,82]

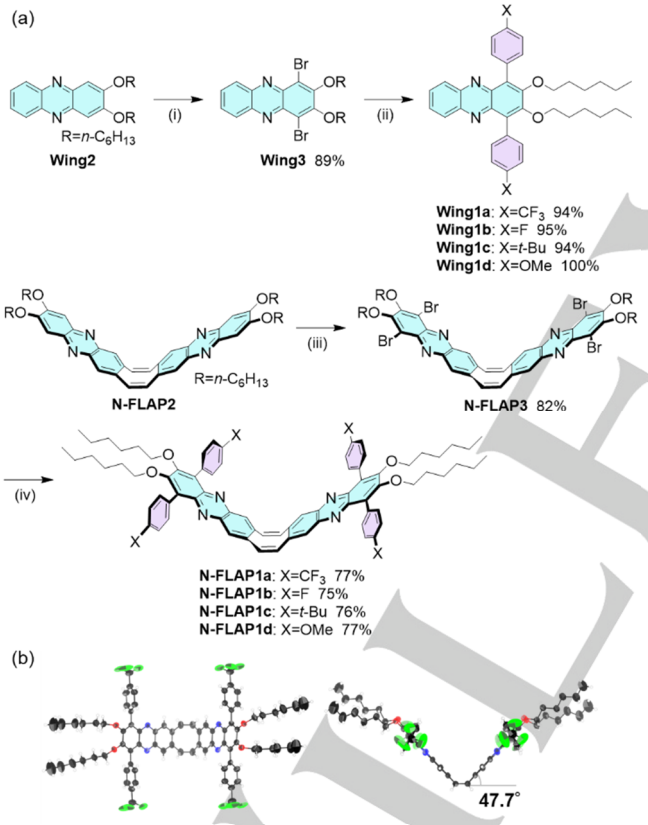

Figure 2. (a) Synthesis of **Wing1a–d** and **N-FLAP1a–d**. Reagents and conditions: (i) *N*-bromosuccinimide (NBS), DMF, 30 °C, 24 h; (ii) arylboronic acid, SPhos Pd G2, K_3PO_4, THF/H_2O, 73 °C, 16 h; (iii) NBS, DMF, 30 °C, 64 h; (iv) arylboronic acid, SPhos Pd G2, K_3PO_4, THF/H_2O, 30 °C, 17 h for **N-FLAP1a**, **N-FLAP1b**, and **N-FLAP1d**, or 22 h for **N-FLAP1c**. (b) X-ray crystal structure of **N-FLAP1a**.

Steady-state fluorescence spectra

Photophysical properties of **Wing1a–d** and **N-FLAP1a–d** were investigated to gain insight into the excited-state conformational changes. The absorption spectra of **Wing1a–d** in dichloromethane (DCM) showed peak maxima at 375–376 nm with the molar absorption coefficients of 1.4–1.6×10^4 mol L^{-1} cm^{-1} (Figure 3a). The lowest-energy absorption band of these spectra underwent a red shift along with the decreasing Hammett's sigma values of the substituents. Furthermore, **Wing1a–d** exhibited broad fluorescence spectra with the full width at half maximum (FWHM) ranging from 3040 to 3190 cm^{-1} and peak tops at 483 nm, 512 nm, 526 nm, and 558 nm, respectively. These broad fluorescence spectra suggested the CT character of **Wing1a–d** between the phenazine core and *para*-substituted phenyl groups. The absorption spectra of **N-FLAP1a–d** in DCM showed a similarity to **Wing1a–d**. The peak maxima were observed at 402–403 nm with the molar absorption coefficients in the range of 3.8–4.0×10^4 mol L^{-1} cm^{-1} (Figure 3b). In addition, the lowest-energy absorption band of these spectra also showed redshifts, reflecting the decreasing Hammett's sigma values of the substituents. While the fluorescence of **N-FLAP1b–d** also exhibited spectral broadening, a unique spectral shape was observed in **N-FLAP1a**, characterized by an overlap of two distinct fluorescence features: a broad band and a relatively sharp spectrum with vibrational progression, which is a hallmark of the fluorescence from the planarized conformation of N-FLAP molecules.[51,54]

Subsequently, the solvent effects on the photophysical properties were also investigated, using cyclohexane, toluene, THF, DCM, and DMF. The absorption spectra of all four **Wing1a–d** compounds showed minimal variation when the solvent was changed (Figure S43). In contrast, the fluorescence spectra showed a red shift as the polarity of solvents increased (Figure S43). The fluorescence peak top (λ_{em}) of **Wing1b** showed a notable red shift from 483 nm (cyclohexane) to 518 nm (DMF) (Figure 3c). This spectral red shift also indicated the CT character in the excited state. As for **N-FLAP1a–d**, the negligible solvent effect on the absorption and the trend of red-shift in the fluorescence by increasing solvent polarity were also observed (Figure S44). In particular, **N-FLAP1a** displayed characteristic fluorescence spectra with clear vibrational progression in these solvents, which indicates the planarization of the COT moiety induced by the ESCE mechanism. In the case of **N-FLAP1b**, the clear vibrational progression was only observed in cyclohexane and toluene (Figure 3d). Since the ESCE state of the FLAP systems is independent of the solvent polarity,[50,51] the red-shifted broad fluorescence spectra in DCM and DMF are assumed to be a similar CT-type emission to **Wing1b**. In other words, the switchable dual emission of **N-FLAP1a–d** was expected by adjusting the CT level of the "wing" part in the excited state. Lippert–Mataga plots for **Wing1a–d** and **N-FLAP1a–d** also showed that the dipole moment difference between the ground and excited states increases as the electron-donating character of the substituents increases (Figure S45, Table S2).

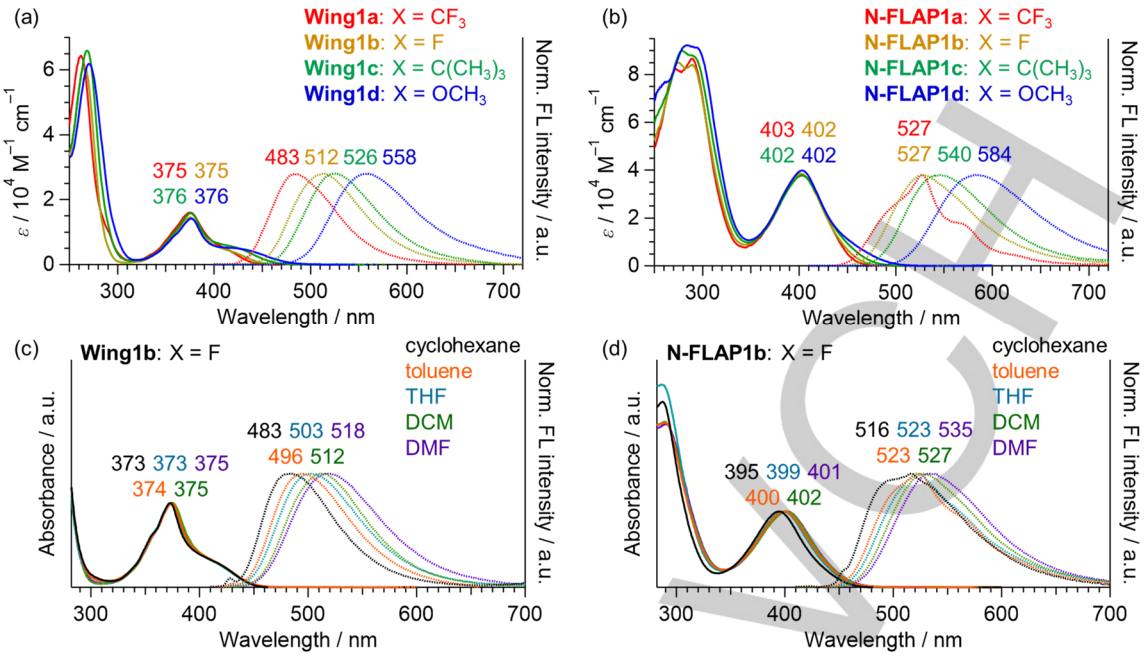

Figure 3. (a,b) Absorption (solid lines) and FL spectra (dotted lines) of (a) **Wing1a–d** and (b) **N-FLAP1a–d** in DCM solution. Fluorescence (FL) spectra were normalized at the peak top. (c,d) Solvent effects on the absorption (solid lines) and FL spectra (dotted lines) of (c) **Wing1b** and (d) **N-FLAP1b**. See Figures S43, S44 for absorption and FL spectra of the other compounds.

Kinetics and thermodynamics in the excited state

Fluorescence quantum yield (Φ_{FL}) and fluorescence lifetime (τ_{FL}) of **Wing1a** were remarkably low in DCM (Φ_{FL} = 0.004, τ_{FL} = 0.1 ns), and the fluorescence is assumed to originate from the CT state. The Φ_{FL} and τ_{FL} values of **Wing1a–d** increased as the substituent's Hammett σ_{para} parameter decreased (Table 1). Among **Wing1a–d**, **Wing1d** showed the largest Φ_{FL} of 0.58 and the longest τ_{FL} of 18 ns in DCM. The radiative decay rate (k_r) of **Wing1a–d** was almost same in DCM (k_r = 0.03–0.04 × 10^9 s^{-1}), while the nonradiative decay rate (k_{nr}) decreased with increasing the Hammett parameter (k_{nr} = 8 × 10^9 s^{-1} for **Wing1a**, k_{nr} = 0.02 × 10^9 s^{-1} for **Wing1d**). Namely, fast nonradiative decay can be dramatically suppressed by the electron-donating ability of the substituents. Since the rapid intersystem crossing (ISC) of the phenazine core has been reported,[83] the nonradiative decay of **Wing1a–d** can be mainly attributed to the ISC from the LE state of the phenazine core. Therefore, a hybridized excited state of the LE and CT states is suggested for **Wing1a–d** (see the paragraph of the theoretical study). Since the emission bands of HLCT and ESCE are overlapped in the fluorescence spectra of **N-FLAP1a–d**, the fluorescence decay analysis was carefully performed. While **Wing1a–d** showed a simple decay profile with a single component, **N-FLAP1a,b** showed a complex decay profile with multiple components of fluorescence lifetime in DCM (Table 2). **N-FLAP1a** exhibited double-component fluorescence decay profile with τ_{FL} < 0.1 ns (65%) and τ_{FL} = 0.3 ns (35%) at λ_{obs} = 485 nm. Although **N-FLAP1b** also exhibited double-component fluorescence decay profile (τ_{FL} = 0.9 and 11 ns), the contribution of the longer lifetime component was quite small (0.07% for τ_{FL} = 11 ns at λ_{obs} = 560 nm), which is consistent with the small spectral area of the ESCE emission band compared with that of HLCT. On the other hand, the fluorescence decay profiles of **N-FLAP1c,d** were fitted basically with a single-component function, and the τ_{FL} values as well as Φ_{FL} were almost same as **Wing1c,d**, respectively. This indicates that the fluorescence from the COT-planarized conformation was not detected in these conditions. These results also demonstrated that switching of dual emission on COT-fused system has been achieved by the substituents.

Table 1. Hammet constant of the substituents, fluorescence quantum yield, and fluorescence lifetime of **Wing1a-d** in DCM. The rate constants of radiative decay and nonradiative decay were also shown.

	σ_{para}[a]	Φ_{FL}[b]	τ_{FL} / ns[c]	k_r / 10^9 s^{-1}	k_{nr} / 10^9 s^{-1}
Wing1a	0.54	0.004	0.1	0.03	8
Wing1b	0.06	0.02	0.6	0.03	2
Wing1c	–0.20	0.06	1.7	0.04	0.6
Wing1d	–0.27	0.58	18	0.03	0.02

[a] Hammett constant from the literature.[84] [b] Excitation λ_{ex} = 380 nm. [c] Excitation λ_{ex} = 405 nm. Observation λ_{obs} = 485 nm (**Wing1a**), 515 nm (**Wing1b**), 525 nm (**Wing1c**), and 560 nm (**Wing1d**).

Table 2. Hammet constant of the substituents, fluorescence quantum yield, and fluorescence lifetime of **N-FLAP1a-d** in DCM. The rate constants of radiative decay and nonradiative decay were also shown.

	σ_{para}[a]	Φ_{FL}[b]	τ_{FL} / ns[c]	k_r / 10^9 s^{-1}	k_{nr} / 10^9 s^{-1}
N-FLAP1a	0.54	0.02	< 0.1 (65%), 0.3 (35%)	–[c]	–[c]
N-FLAP1b	0.06	0.03	0.9 (> 99%), 11 (0.07%)	–[c]	–[c]
N-FLAP1c	–0.20	0.08	2.3	0.03	0.4
N-FLAP1d	–0.27	0.58	21	0.03	0.02

[a] Hammett constant from the literature.[84] [b] Excitation λ_{ex} = 400 nm. [c] Excitation λ_{ex} = 405 nm. Observation λ_{obs} = 480 nm (**N-FLAP1a**), 560 nm (**N-FLAP1b**), 570 nm (**N-FLAP1c**), and 560 nm (**N-FLAP1d**). [c] Decay constants were not able to be estimated from the double-component decay profile.

Solvent effects were also examined. Taking **Wing1b** as an example (Table 3), Φ_{FL} increased and τ_{FL} got longer by increasing the polarity of the solvent from cyclohexane (ε_r = 2.02; Φ_{FL} = 0.004, τ_{FL} = 0.1 ns) to DMF (ε_r = 36.71; Φ_{FL} = 0.02, τ_{FL} = 0.6 ns). While k_r is almost constant (k_r = 0.03–0.04×10^9 s^{-1}), k_{nr} decreased with increasing solvent polarity (k_{nr} = 1×10^{10} s^{-1} in cyclohexane, k_{nr} = 2×10^9 s^{-1} in DMF). A similar trend was observed for **Wing1a**, **Wing1c**, and **Wing1d** (see Figure S46 and Table S3). Also for **N-FLAP1a–d**, the Φ_{FL} and τ_{FL} values increased in polar solvents (Table 4, Figures S47–S50, and Table S4). The longer lifetime would be induced by changing the energy level of the HLCT state in S_1, causing slower ISC (see below). The ISC behavior of **N-FLAP1a–d** appears to be different from that of **N-FLAP2**.[85]

Table 3. Fluorescence quantum yield (Φ_{FL}) and fluorescence lifetime (τ_{FL}) of **Wing1b** in solvents with various relative permittivity (ε_r). Calculated rate constants of radiative decay (k_r) and non-radiative decay (k_{nr}) are also shown.

Solvent	ε_r	Φ_{FL}[a]	τ_{FL} / ns[b]	k_r / 10^9 s^{-1}	k_{nr} / 10^9 s^{-1}
cyclohexane	2.02	0.004	0.1	0.04	1×10
toluene	2.38	0.007	0.2	0.04	6
THF	7.58	0.009	0.2	0.04	4
DCM	8.93	0.02	0.6	0.03	2
DMF	36.71	0.02	0.6	0.04	2

[a] Excitation λ_{ex} = 380 nm. [b] Excitation λ_{ex} = 405 nm. Observation λ_{obs} = 490 nm (cyclohexane), 510 nm (toluene), 510 nm (THF), 525 nm (DCM), and 530 nm (DMF).

Table 4. Fluorescence quantum yield (Φ_{FL}) and fluorescence lifetime (τ_{FL}) of **N-FLAP1d** in solvents with various relative permittivity (ε_r). Calculated rate constants of radiative decay (k_r) and non-radiative decay (k_{nr}) are also shown.

Solvent	ε_r	Φ_{FL}[a]	τ_{FL} / ns[b]	k_r / 10^9 s^{-1}	k_{nr} / 10^9 s^{-1}
cyclohexane	2.02	0.06	1.4	0.04	0.7
toluene	2.38	0.21	5.4	0.04	0.1
THF	7.58	0.36	12	0.03	0.05
DCM	8.93	0.58	21	0.03	0.02
DMF	36.71	0.50	20	0.03	0.03

[a] Excitation λ_{ex} = 400 nm. [b] Excitation λ_{ex} = 405 nm. Observation λ_{obs} = 500 nm (cyclohexane), 540 nm (toluene), 560 nm (THF), 560 nm (DCM), and 580 nm (DMF).

The activation energy (E_a) and enthalpy gap (ΔH) of the bent-to-planar conformational change of **N-FLAP1a,b** in S_1 were determined by the Stevens-Ban plot based on variable temperature fluorescence spectroscopy in toluene (Figure 4).[39,53,86] The E_a barrier from the bent HLCT state to the planar ESCE states in **N-FLAP1a** and **N-FLAP1b** were determined to be 4.9 and 2.4 kcal/mol, respectively. The ΔH values were also estimated to be –1.8 and –0.9 kcal/mol, respectively. The tendency of smaller activation energy with decreasing enthalpy gap is inconsistent with the Bell–Evans–Polanyi principle in S_1, unlike the reported example.[67] Namely, the excited state dynamics cannot be fully interpreted by the simple two-state model in S_1, and therefore the involvement of the ISC process to triplet excited states is again predicted. Regarding **N-FLAP1c**, the contribution of ESCE in the fluorescence spectrum was too small to estimate (Figure S53c), probably because E_a is higher than that of **N-FLAP1a** and **N-FLAP1b**.

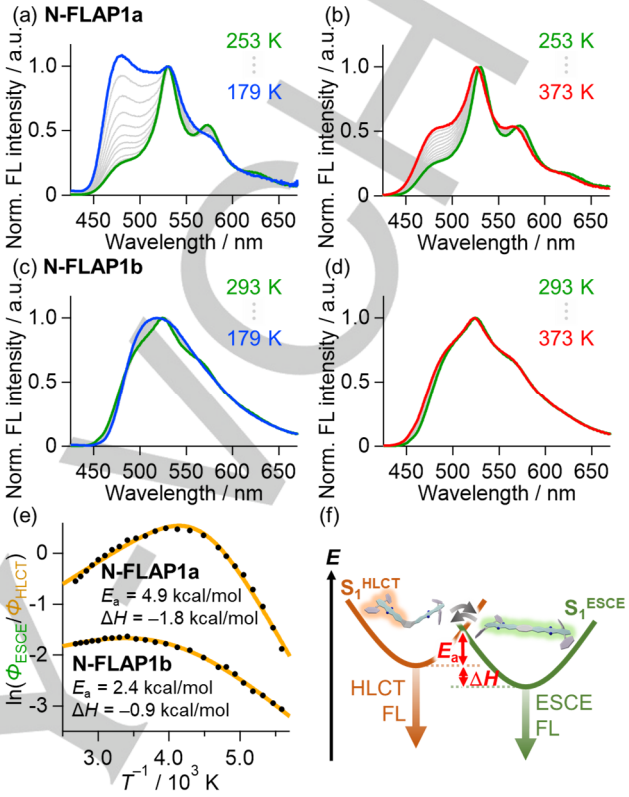

Figure 4. (a–d) Variable temperature FL spectra of (a,b) **N-FLAP1a** and (c,d) **N-FLAP1b**. (e) Stevens-Ban plot of **N-FLAP1a** and **N-FLAP1b**. The activation energy (E_a) and enthalpy gap (ΔH) between the bent and planar conformations in S_1 were estimated. See Figure S54 in detail. (f) Dual FL from the bent HLCT and planar ESCE states, observed in **N-FLAP1a** and **N-FLAP1b**.

When dispersed in a polymethyl methacrylate (PMMA) matrix, **Wing1a–d** as well as **N-FLAP1a–d** showed a blue shift of the fluorescence compared to those spectra in DCM (Figure S51). Rotation of the aryl substituents would be partially suppressed in the rigid polymer matrix. Furthermore, the vibrational progression of **N-FLAP1a** disappeared when doped in a PMMA matrix, indicating that the planarization of the COT ring is almost suppressed (Figure S51b).[51] The fluorescence decay profiles of **Wing1a–d** and **N-FLAP1a–d** were more complex than those in solution (Figure S52 and Table S7).

Fast intersystem crossing revealed by transient absorption spectroscopy

To investigate the excited-state dynamics in more detail, transient absorption (TA) spectra of **Wing1a**,**d** and **N-FLAP1a**,**d** in DCM were measured using an excitation pulse centered at 400 nm. Immediately after photoexcitation, the TA spectra of **Wing1a** showed a broad excited-state absorption (ESA) band (Figure 5a). On a sub-ps time scale, the overall signal intensity of this ESA band increased, which can be assigned to the relaxation from the initially populated high-lying excited state (S_n) to S_1.

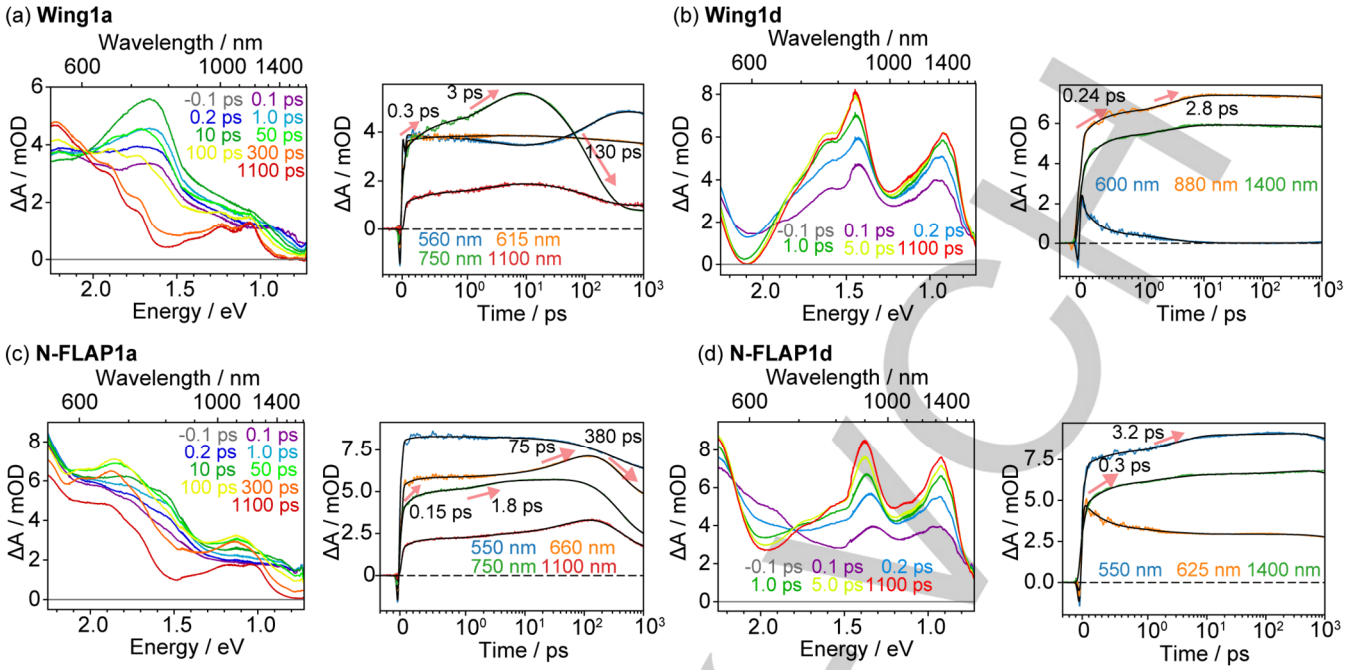

Figure 5. Transient absorption spectra and temporal profiles of (a) **Wing1a**, (b) **Wing1d**, (c) **N-FLAP1a**, and (d) **N-FLAP1d** in DCM. The time axis is linear in the -0.3 to 1.0 ps range and logarithmic for later delay times.

Subsequently, a further spectral change was observed on the picosecond time scale, characterized by the growth of the ESA signal around 750 nm. This process is assignable to the structural relaxation of **Wing1a** in S_1, likely involving the rotation of the aryl substituents on the phenazine core. The band at around 750 nm then decayed with a time constant of 130 ps, leaving the ESA band peaked at 560 nm as the predominant feature. This time constant is in good agreement with τ_{FL} of **Wing1a** (≈ 0.1 ns), suggesting that the 130-ps component corresponds to the ISC process. The observation of an isosbestic point at 615 nm in the time range of 10–300 ps (Figure S58) indicates that the ISC occurs from the equilibrated S_1. The fast ISC is consistent with the low Φ_{FL} of **Wing1a**.

The TA dynamics of **Wing1d** is similar to that of **Wing1a** at early delay times (Figure 5b), showing sub-ps signal growth and subsequent spectral change on the picosecond time scale. As in the case of **Wing1a**, these features can be assigned to the relaxation from the high-lying excited state (S_n) and structural changes in S_1, respectively. On the other hand, in contrast to **Wing1a**, the TA spectral features of **Wing1d** did not change significantly after 5 ps, indicating the absence of the ISC process. This interpretation is consistent with the long τ_{FL} (18 ns) and high Φ_{FL} (0.58) of **Wing1d**.

N-FLAP1a exhibited more complex dynamics, as shown in Figure 5c. On the femtosecond to picosecond time scale, its dynamics is similar to that observed in **Wing1a**. However, on longer time scales, **N-FLAP1a** showed more complex behavior, characterized by time constants of 75 and 380 ps, along with a long-lived species (>1 ns). The spectrum of the long-lived species closely resembles that of **Wing1a**, allowing it to be assigned to the triplet state. This similarity in the spectral shape also suggests that the triplet state takes a V-shaped conformation and is formed from the bent HLCT state. The 380-ps time constant is comparable to the second component of τ_{FL} of **N-FLAP1a** (0.3 ns, Table 2), and thus, we attribute this component to the ESCE state formed from the HLCT state by the COT planarization. Accordingly, we assign the 75-ps time constant to the lifetime of S_1, which yields the triplet state and ESCE state in parallel by the ISC and COT planarization, respectively. In contrast to **N-FLAP1a**, **N-FLAP1d** exhibited simpler dynamics (Figure 5d). The TA spectra and dynamics of **N-FLAP1d** are almost the same as **Wing1d**. As a result, the suppression of the COT planarization and the electronically insulated phenazine moieties in the bent HLCT state were again indicated in **N-FLAP1d** (Figure 5b,d). The dynamics of each sample derived from the transient absorption data are summarized in Figure S60.

Computational interpretation of excited state dynamics

The energy levels of the excited states were estimated by DFT calculations using the Gaussian 16 package[87]. Model structures **Wing1a′–d′** bearing methyl groups instead of *n*-hexyl groups were calculated (Figure S61). The cam-B3LYP functional was selected because this functional is suitable to treat long-range CT transitions.[88] The conductor-like polarizable continuum model (CPCM)[89] of DCM was used for the following calculations. The torsion angle between the phenazine skeleton and the *para*-substituted phenyl groups (Figure S62) of **Wing1a′–d′** were calculated to be 53.6–55.4° in S_0, and these angles decreased to 38.8–41.3° in S_1. The configuration of S_1 was mainly composed of a CT character in **Wing1a′–d′**. The NTO analysis[90] was performed to quantify the degree of local excitation and charge transfer excitation (Figures 6a).

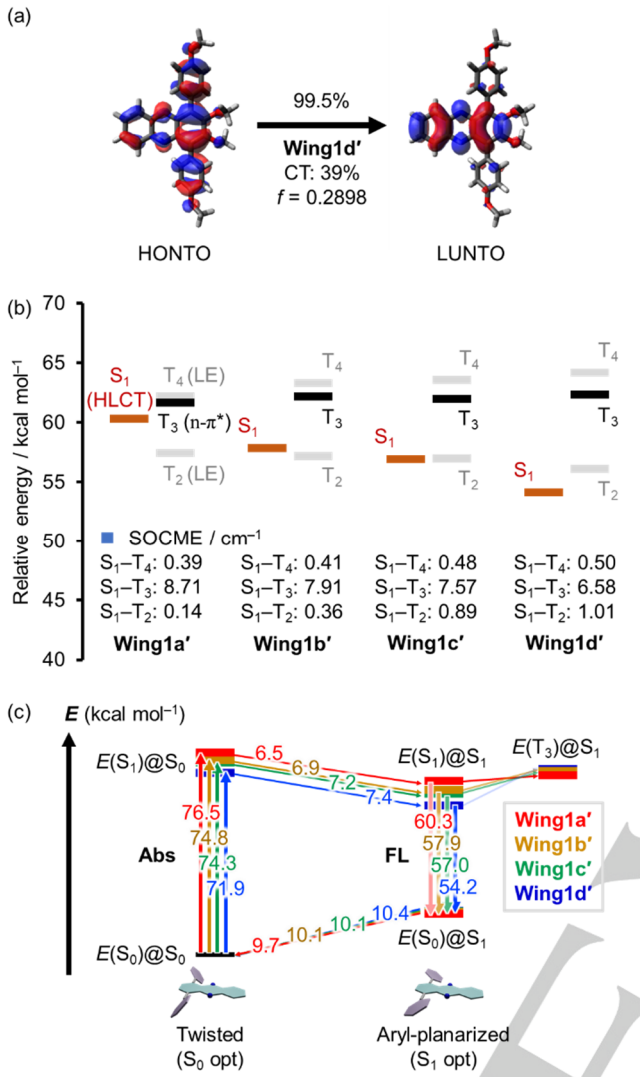

Figure 6. DFT calculations of **Wing1a′-d′** at the (TD)-cam-B3LYP/def2-TZVP/CPCM(DCM)//(TD)-cam-B3LYP/def2-SVP/CPCM(DCM) level of theory. (a) HONTO and LUNTO of **Wing1d′**. Occupancy of the NTOs and the calculated %CT with oscillator strengths are shown above and below the arrows, respectively. (b) Energy levels of S_1 and triplet excited states and SOCME between the states calculated at the S_1 optimized geometries. (c) Relative energy levels the $S_0/S_1/T_3$ states at the twisted/aryl-planarized conformations for **Wing1a′-d′**. The energy gap between states is shown in kcal mol^{-1}.

The highest occupied natural transition orbital (HONTO) of **Wing1a′–d′** demonstrated an effective hybridization between HOMO of phenazine and HOMO of *para*-terphenyl. Proportion of the CT state (%CT) was evaluated using Multiwfn 3.8 software.[91] In the case of **Wing1a′**, %CT is calculated to be 23%, and %CT increased by decreasing Hamett parameter. **Wing1d′** showed the highest %CT (39%) among **Wing1a′–d′**. In other words, electron-donating ability of the aryl substituents enhances the CT character from the aryl groups to the phenazine core. The oscillator strengths at the optimized geometries of **Wing1a′–d′** in S_1 were calculated to be f = 0.24–0.29, which is relatively high due to the hybridization of LE and CT states.

Regarding **Wing1a′–d′**, the energy levels of S_1 and triplet excited states (T_1–T_4) were calculated, and the spin-orbit coupling matrix element (SOCME) was estimated using the ORCA 5.0.4 package[92] (Figure 6b). There are several triplet energy levels near S_1, while T_1 is quite lower than S_1 (Table S14). This trend is typical of the HLCT fluorophores.[72] Configurations of T_2 and T_4 are explained as local excited states (LE) of the phenazine core, and that of T_3 as n-π^* excited state of the phenazine core. The SOCME values of the S_1 to T_3 transition (7.57–8.71 cm^{-1}) were much higher than those of the S_1 to T_2 transition (0.14–1.01 cm^{-1}) and the S_1 to T_4 transition (0.39–0.50 cm^{-1}), which is consistent with the El-Sayed rule.[93,94] Due to the decreased S_1 level, the calculated energy gap between S_1 to T_3 significantly increased in **Wing1d′** (Figure 6c), which explains the suppression of ISC observed in TA spectroscopy of **Wing1d** as well as the red-shifted fluorescence with high Φ_{FL} and long τ_{FL}.

In the case of **N-FLAP1a′–d′**, the triplet excited state with n-π^* configuration was identified to be T_5 at this level of theory (Figure 7), and the SOCME values for the HLCT to T_5(n-π^*) transition were calculated to be 6.74–8.86 cm^{-1} (Table S16). These calculations supported a similar trend to **Wing1a′–d′**. Namely, the ISC process was significant in **N-FLAP1a** (low Φ_{FL} and short τ_{FL}), while it was suppressed in **N-FLAP1d** (high Φ_{FL} and long τ_{FL}). The calculations are also consistent with the observed energy shifts in the lowest-energy absorption band and the fluorescence band (Figure 3b). The difference of the FLAP molecules from the Wing structures is the involvement of the COT planarization dynamics to the ESCE state, but it has been only explicit in **N-FLAP1a** and **N-FLAP1b** because of the small energy barrier from HLCT to ESCE. The calculation on the ESCE state also agreed with the experiments (see SI).

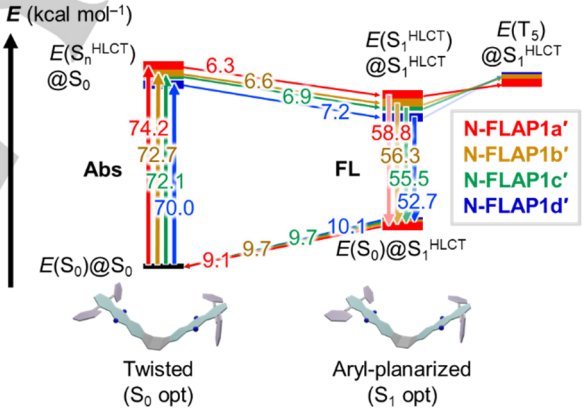

Figure 7. Relative energy levels of the $S_0/S_1/T_n$ states at multiple conformations of **N-FLAP1a′-d′** at the twisted/aryl-planarized conformations. Geometry optimization was performed at the (TD)-cam-B3LYP/def2-SVP/CPCM(DCM) level of theory, and the energy calculations at the TD-cam-B3LYP/def2-TZVP/CPCM(DCM) level. The energy gap is shown in kcal mol^{-1}.

Conclusion

In conclusion, we have developed a series of novel fluorescent molecules that show dual emission from the HLCT and ESCE states. Combination of the phenazine core and the *para*-substituted phenyl groups provided **Wing1a–d**, which exhibited a hybridized LE and CT character, classified as an HLCT moiety. The energy-tunable HLCT excited state of the skeleton was adopted as the “flapping wings” of the COT-fused system to develop a new FLAP molecule that shows a characteristic dual emission from the HLCT state as well as the inherent ESCE state

of the planarized COT geometry. Excited state dynamics were investigated with the TA measurements. As a result, the rapid intersystem crossing was indicated for the FLAP molecule with an electron-withdrawing substituent, **N-FLAP1a**, which showed a faint dual emission from the bent HLCT and the planar ESCE states with low Φ_{FL} and short τ_{FL}. The emission wavelength of the HLCT state can be tuned by changing the solvent. On the other hand, the FLAP molecule with an electron-donating group, **N-FLAP1d**, showed an almost same trend to the corresponding Wing molecule, **Wing1d**, which showed a single-component bright fluorescence from the HLCT state with high Φ_{FL} and long τ_{FL}. These behaviors are fully interpreted by TD-DFT calculations on the excited state energy levels and the estimation of the spin-orbit coupling between singlet and triplet excited states. This study revealed the push-pull effects on the photophysical properties of the N-FLAP molecules, which led to the development of the dual emissive fluorophores with a new mechanism combined with HLCT and ESCE.

Experimental Section

Details for synthesis, X-ray structure analysis, photophysical properties, transient absorption spectroscopy, and quantum chemical calculations can be found in the Supporting Information.

Acknowledgement

This work was supported by JST FOREST Program (JPMJFR201K and JPMJFR201L), JSPS KAKENHI (JP21H01895 and JP24H00473), JSPS Fellowship (JP22KJ1964), and the Asahi Glass Foundation. We thank Prof. Hideki Yorimitsu (Kyoto University) for his help with high-resolution mass spectrometry measurements. We also thank Mr. Katsuki Miyokawa and Dr. Tatsuhiko Yoshino (Kyoto University) for their spot-on advice in quantum chemical calculations. Part of computation time was provided by the SuperComputer System, Institute for Chemical Research, Kyoto University.

Keywords: Charge transfer • Conformational change • Dual emission • Excited state • Fluorescence

References

[1] S. K. Behera, S. Y. Park, J. Gierschner, *Angew. Chem. Int. Ed.* **2021**, *60*, 22624–22638.
[2] R. Gui, H. Jin, X. Bu, Y. Fu, Z. Wang, Q. Liu, *Coord. Chem. Rev.* **2019**, *383*, 82–103.
[3] A. S. Klymchenko, *Acc. Chem. Res.* **2017**, *50*, 366–375.
[4] A. Bigdeli, F. Ghasemi, S. Abbasi-Moayed, M. Shahrajabian, N. Fahimi-Kashani, S. Jafarinejad, M. A. Farahmand Nejad, M. R. Hormozi-Nezhad, *Anal. Chim. Acta* **2019**, *1079*, 30–58.
[5] M. A. Haidekker, E. A. Theodorakis, *J. Mater. Chem. C* **2016**, *4*, 2707–2718.
[6] S.-H. Park, N. Kwon, J.-H. Lee, J. Yoon, I. Shin, *Chem. Soc. Rev.* **2020**, *49*, 143–179.
[7] M. H. Lee, J. S. Kim, J. L. Sessler, *Chem. Soc. Rev.* **2015**, *44*, 4185–4191.
[8] L.-Y. Niu, Y.-Z. Chen, H.-R. Zheng, L.-Z. Wu, C.-H. Tung, Q.-Z. Yang, *Chem. Soc. Rev.* **2015**, *44*, 6143–6160.
[9] Q. Zhao, F. Li, C. Huang, *Chem. Soc. Rev.* **2010**, *39*, 3007–3030.
[10] M. K. Kuimova, *Phys. Chem. Chem. Phys.* **2012**, *14*, 12671–12686.
[11] A. Bednarkiewicz, J. Drabik, K. Trejgis, D. Jaque, E. Ximendes, L. Marciniak, *Appl. Phys. Rev.* **2021**, *8*, 011317.
[12] X. Hu, Y. Li, T. Liu, G. Zhang, S. Liu, *ACS Appl. Mater. Interfaces* **2015**, *7*, 15551–15560.
[13] S. Bassnett, L. Reinisch, D. C. Beebe, *Am. J. Physiol.* **1990**, *258*, C171-8.
[14] C. Matellan, A. E. Del Río Hernández, *ACS Biomater. Sci. Eng.* **2019**, *5*, 3703−3719.
[15] Y. Liu, K. Galior, V. P.-Y. Ma, K. Salaita, *Acc. Chem. Res.* **2017**, *50*, 2915–2924.
[16] V. P.-Y. Ma, Y. Liu, L. Blanchfield, H. Su, B. D. Evavold, K. Salaita, *Nano Lett.* **2016**, *16*, 4552–4559.
[17] M. Tian, Y. Ma, W. Lin, *Acc. Chem. Res.* **2019**, *52*, 2147–2157.
[18] X. Huang, J. Song, B. C. Yung, X. Huang, Y. Xiong, X. Chen, *Chem. Soc. Rev.* **2018**, *47*, 2873–2920.
[19] H. V. Humeniuk, A. Rosspeintner, G. Licari, V. Kilin, L. Bonacina, E. Vauthey, N. Sakai, S. Matile, *Angew. Chem. Int. Ed.* **2018**, *57*, 10559–10563.
[20] J. Zhang, R. E. Campbell, A. Y. Ting, R. Y. Tsien, *Nat. Rev. Mol. Cell Biol.* **2002**, *3*, 906–918.
[21] E. M. Lloyd, J. R. Vakil, Y. Yao, N. R. Sottos, S. L. Craig, *J. Am. Chem. Soc.* **2023**, *145*, 751–768.
[22] D. Kim, M. S. Kwon, C. W. Lee, *Polym. Chem.* **2022**.
[23] J. Li, C. Nagamani, J. S. Moore, *Acc. Chem. Res.* **2015**, *48*, 2181–2190.
[24] C. L. Brown, S. L. Craig, *Chem. Sci.* **2015**, *6*, 2158–2165.
[25] B. R. Crenshaw, C. Weder, *Chem. Mater.* **2003**, *15*, 4717–4724.
[26] I. E. Steinmark, A. L. James, P.-H. Chung, P. E. Morton, M. Parsons, C. A. Dreiss, C. D. Lorenz, G. Yahioglu, K. Suhling, *PLoS One* **2019**, *14*, e0211165.
[27] W. Becker, *J. Microsc.* **2012**, *247*, 119–136.
[28] C. Grashoff, B. D. Hoffman, M. D. Brenner, R. Zhou, M. Parsons, M. T. Yang, M. A. McLean, S. G. Sligar, C. S. Chen, T. Ha, M. A. Schwartz, *Nature* **2010**, *466*, 263–266.
[29] J. R. Lakowicz, H. Szmacinski, K. Nowaczyk, K. W. Berndt, M. Johnson, *Anal. Biochem.* **1992**, *202*, 316–330.
[30] F. Meng, T. M. Suchyna, F. Sachs, *FEBS J.* **2008**, *275*, 3072–3087.
[31] L. Liu, F. He, Y. Yu, Y. Wang, *Front. Bioeng. Biotechnol.* **2020**, *8*, 595497.
[32] Y. Wang, N. Wang, *Integr. Biol.* **2009**, *1*, 565–573.
[33] A. C. Sedgwick, L. Wu, H.-H. Han, S. D. Bull, X.-P. He, T. D. James, J. L. Sessler, B. Z. Tang, H. Tian, J. Yoon, *Chem. Soc. Rev.* **2018**, *47*, 8842–8880.
[34] Z. N. Scheller, D. Liese, H. Siera, N. Semleit, M. Schmiedtchen, C. Wölper, G. Haberhauer, *Chem. Eur. J* **2024**, *30*, e202304143.
[35] Y. Mu, L. Liao, W. Li, Z. Yang, Y. Zhang, Y. Huo, Z. Chi, *Chem. Eur. J.* **2023**, *29*, e202300867.
[36] C. Wang, W. Chi, Q. Qiao, D. Tan, Z. Xu, X. Liu, *Chem. Soc. Rev.* **2021**, *50*, 12656–12678.
[37] S. Sasaki, G. P. C. Drummen, G.-I. Konishi, *J. Mater. Chem. C* **2016**, *4*, 2731–2743.
[38] G. Haberhauer, R. Gleiter, C. Burkhart, *Chem. Eur. J.* **2016**, *22*, 971–978.
[39] Z. R. Grabowski, K. Rotkiewicz, W. Rettig, *Chem. Rev.* **2003**, *103*, 3899–4032.
[40] H. Osaki, C.-M. Chou, M. Taki, K. Welke, D. Yokogawa, S. Irle, Y. Sato, T. Higashiyama, S. Saito, A. Fukazawa, S. Yamaguchi, *Angew. Chem. Int. Ed.* **2016**, *55*, 7131–7135.
[41] J. Gierschner, H.-G. Mack, D. Oelkrug, I. Waldner, H. Rau, *J. Phys. Chem. A* **2004**, *108*, 257–263.
[42] F. M. Winnik, *Chem. Rev.* **1993**, *93*, 587–614.
[43] S. Qiu, Z. Zhang, Z. Wang, D.-H. Qu, H. Tian, *Precision Chemistry* **2023**, *1*, 129–138.

[44] Z. Zong, Q. Zhang, S.-H. Qiu, Q. Wang, C. Zhao, C.-X. Zhao, H. Tian, D.-H. Qu, *Angew. Chem. Int. Ed.* **2022**, *61*, e202116414.
[45] P. Emele, D. U. Meyer, N. Holl, H. Port, H. C. Wolf, F. Würthner, P. Bäuerle, F. Effenberger, *Chem. Phys.* **1994**, *181*, 417–424.
[46] P. Valat, V. Wintgens, J. Kossanyi, L. Biczok, A. Demeter, T. Berces, *J. Am. Chem. Soc.* **1992**, *114*, 946–953.
[47] C. Yuan, S. Saito, C. Camacho, S. Irle, I. Hisaki, S. Yamaguchi, *J. Am. Chem. Soc.* **2013**, *135*, 8842–8845.
[48] K. Suga, T. Yamakado, S. Saito, *Bull. Chem. Soc. Jpn* **2021**, *94*, 1999–2002.
[49] R. Kimura, H. Kuramochi, P. Liu, T. Yamakado, A. Osuka, T. Tahara, S. Saito, *Angew. Chem. Int. Ed.* **2020**, *59*, 16430–16435.
[50] R. Kotani, H. Sotome, H. Okajima, S. Yokoyama, Y. Nakaike, A. Kashiwagi, C. Mori, Y. Nakada, S. Yamaguchi, A. Osuka, A. Sakamoto, H. Miyasaka, S. Saito, *J. Mater. Chem. C* **2017**, *5*, 5248–5256.
[51] Y. Goto, S. Omagari, R. Sato, T. Yamakado, R. Achiwa, N. Dey, K. Suga, M. Vacha, S. Saito, *J. Am. Chem. Soc.* **2021**, *143*, 14306–14313.
[52] R. Kotani, S. Yokoyama, S. Nobusue, S. Yamaguchi, A. Osuka, H. Yabu, S. Saito, *Nat. Commun.* **2022**, *13*, 303.
[53] T. Yamakado, S. Saito, *J. Am. Chem. Soc.* **2022**, *144*, 2804–2815.
[54] K. Suga, T. Yamakado, S. Saito, *J. Am. Chem. Soc.* **2023**, *145*, 26799–26809.
[55] G. Sun, Y.-C. Wei, Z. Zhang, J.-A. Lin, Z.-Y. Liu, W. Chen, J. Su, P.-T. Chou, H. Tian, *Angew. Chem. Int. Ed.* **2020**, *59*, 18611–18618.
[56] B. Shao, H. Qian, Q. Li, I. Aprahamian, *J. Am. Chem. Soc.* **2019**, *141*, 8364–8371.
[57] D. Bléger, J. Schwarz, A. M. Brouwer, S. Hecht, *J. Am. Chem. Soc.* **2012**, *134*, 20597–20600.
[58] A. A. Beharry, O. Sadovski, G. A. Woolley, *J. Am. Chem. Soc.* **2011**, *133*, 19684–19687.
[59] S. Yang, C.-X. Zhao, S. Crespi, X. Li, Q. Zhang, Z.-Y. Zhang, J. Mei, H. Tian, D.-H. Qu, *Chem* **2021**, *7*, 1544–1556.
[60] Z. Zhang, C.-L. Chen, Y.-A. Chen, Y.-C. Wei, J. Su, H. Tian, P.-T. Chou, *Angew. Chem. Int. Ed.* **2018**, *57*, 9880–9884.
[61] W. Chen, C.-L. Chen, Z. Zhang, Y.-A. Chen, W.-C. Chao, J. Su, H. Tian, P.-T. Chou, *J. Am. Chem. Soc.* **2017**, *139*, 1636–1644.
[62] Z. Zhang, Y.-S. Wu, K.-C. Tang, C.-L. Chen, J.-W. Ho, J. Su, H. Tian, P.-T. Chou, *J. Am. Chem. Soc.* **2015**, *137*, 8509–8520.
[63] S. Fukumoto, T. Nakashima, T. Kawai, *Angew. Chem. Int. Ed.* **2011**, *50*, 1565–1568.
[64] Y. Kishimoto, J. Abe, *J. Am. Chem. Soc.* **2009**, *131*, 4227–4229.
[65] R. Siewertsen, H. Neumann, B. Buchheim-Stehn, R. Herges, C. Näther, F. Renth, F. Temps, *J. Am. Chem. Soc.* **2009**, *131*, 15594–15595.
[66] R. Kotani, L. Liu, P. Kumar, H. Kuramochi, T. Tahara, P. Liu, A. Osuka, P. B. Karadakov, S. Saito, *J. Am. Chem. Soc.* **2020**, *142*, 14985–14992.
[67] Y. Chen, K.-H. Chang, F.-Y. Meng, S.-M. Tseng, P.-T. Chou, *Angew. Chem. Int. Ed.* **2021**, *60*, 7205–7212.
[68] Y. Chen, S.-M. Tseng, K.-H. Chang, P.-T. Chou, *J. Am. Chem. Soc.* **2022**, *144*, 1748–1757.
[69] X. Sun, M. Cong, X. Jin, J. Su, Z. Zhang, *J. Phys. Chem. C Nanomater. Interfaces* **2024**, *128*, 15124–15131.
[70] J.-M. Ji, H. Zhou, H. K. Kim, *J. Mater. Chem. A* **2018**, *6*, 14518–14545.
[71] W. Li, D. Liu, F. Shen, D. Ma, Z. Wang, T. Feng, Y. Xu, B. Yang, Y. Ma, *Adv. Funct. Mater.* **2012**, *22*, 2797–2803.
[72] W. Li, Y. Pan, L. Yao, H. Liu, S. Zhang, C. Wang, F. Shen, P. Lu, B. Yang, Y. Ma, *Adv. Opt. Mater.* **2014**, *2*, 892–901.
[73] Y. Pan, J. Huang, W. Li, Y. Gao, Z. Wang, D. Yu, B. Yang, Y. Ma, *RSC Adv.* **2017**, *7*, 19576–19583.
[74] T. Jairam, W. P. Hong, *J. Mater. Chem. C* **2022**, *10*, 16173–16217.
[75] Q. Wei, N. Fei, A. Islam, T. Lei, L. Hong, R. Peng, X. Fan, L. Chen, P. Gao, Z. Ge, *Adv. Opt. Mater.* **2018**, *6*, 1800512.
[76] Q. Luo, L. Li, H. Ma, C. Lv, X. Jiang, X. Gu, Z. An, B. Zou, C. Zhang, Y. Zhang, *Chem. Sci.* **2020**, *11*, 6020–6025.
[77] X. Li, Y. Lv, S. Chang, H. Liu, W. Mo, H. Ma, C. Zhou, S. Zhang, B. Yang, *Anal. Chem.* **2019**, *91*, 10927–10931.
[78] B. Li, L. Zhou, H. Cheng, Q. Huang, J. Lan, L. Zhou, J. You, *Chem. Sci.* **2018**, *9*, 1213–1220.
[79] Q. Huang, Q. Guo, J. Lan, J. You, *Dyes Pigm.* **2021**, *193*, 109497.
[80] R. B. Kanth Siram, J. Smith, T. D. Anthopoulos, S. Patil, *J. Mater. Chem.* **2012**, *22*, 4450–4458.
[81] Y. Li, Y. Fu, H. Tong, Z. Xie, L. Wang, *J. Polym. Sci. A Polym. Chem.* **2013**, *51*, 2910–2918.
[82] C. Yuan, S. Saito, C. Camacho, T. Kowalczyk, S. Irle, S. Yamaguchi, *Chem. Eur. J.* **2014**, *20*, 2193–2200.
[83] Y. Hirata, I. Tanaka, *Chem. Phys. Lett.* **1976**, *43*, 568–570.
[84] C. Hansch, A. Leo, R. W. Taft, *Chem. Rev.* **1991**, *91*, 165–195.
[85] S. Paul, H. Kitakado, K. Suga, R. Kotani, N. Dey, E. Matito, R. Venkatramani, S. Saito, J. Dasgupta, *J. Mater. Chem. C* **2023**, *11*, 12243–12253.
[86] B. Stevens, M. I. Ban, *Trans. Faraday Soc.* **1964**, *60*, 1515.
[87] M. J. Frisch, G. W. Trucks, H. B. Schlegel, G. E. Scuseria, M. A. Robb, J. R. Cheeseman, G. Scalmani, V. Barone, G. A. Petersson, H. Nakatsuji, X. Li, M. Caricato, A. V. Marenich, J. Bloino, B. G. Janesko, R. Gomperts, B. Mennucci, H. P. Hratchian, J. V. Ortiz, A. F. Izmaylov, J. L. Sonnenberg, D. Williams-Young, F. Ding, F. Lipparini, F. Egidi, J. Goings, B. Peng, A. Petrone, T. Henderson, D. Ranasinghe, V. G. Zakrzewski, J. Gao, N. Rega, G. Zheng, W. Liang, M. Hada, M. Ehara, K. Toyota, R. Fukuda, J. Hasegawa, M. Ishida, T. Nakajima, Y. Honda, O. Kitao, H. Nakai, T. Vreven, K. Throssell, J. A. Montgomery Jr, J. E. Peralta, F. Ogliaro, M. J. Bearpark, J. J. Heyd, E. N. Brothers, K. N. Kudin, V. N. Staroverov, T. A. Keith, R. Kobayashi, J. Normand, K. Raghavachari, A. P. Rendell, J. C. Burant, S. S. Iyengar, J. Tomasi, M. Cossi, J. M. Millam, M. Klene, C. Adamo, R. Cammi, J. W. Ochterski, R. L. Martin, K. Morokuma, O. Farkas, J. B. Foresman, D. J. Fox, *Gaussian 16, Revision C.02, Gaussian, Inc., Wallingford*, **2016**.
[88] T. Yanai, D. P. Tew, N. C. Handy, *Chem. Phys. Lett.* **2004**, *393*, 51–57.
[89] M. Cossi, N. Rega, G. Scalmani, V. Barone, *J. Comput. Chem.* **2003**, *24*, 669–681.
[90] R. L. Martin, *J. Chem. Phys.* **2003**, *118*, 4775–4777.
[91] T. Lu, F. Chen, *J. Comput. Chem.* **2012**, *33*, 580–592.
[92] F. Neese, *Wiley Interdiscip. Rev. Comput. Mol. Sci.* **2012**, *2*, 73–78.
[93] M. A. El-Sayed, *Acc. Chem. Res.* **1968**, *1*, 8–16.
[94] S. E. Braslavsky, *Pure Appl. Chem.* **2007**, *79*, 293–465.

Entry for the Table of Contents

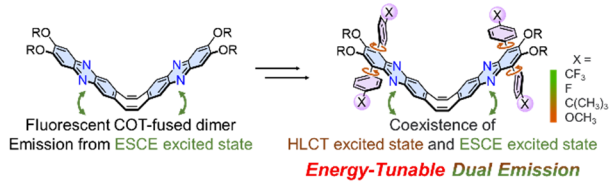

A series of dual-fluorescent molecules involving a hybridized local and charge-transfer (HLCT) excited state with the excited-state conjugation enhancement (ESCE) motif has been reported as the first case. The energy level of the HLCT state has been adjusted by modulating substituents and solvents, separately from the ESCE energy level, proposing a new strategy for the development of advanced fluorescent probes.

Institute and/or researcher Twitter usernames: @sugachemsuke